Magneto-optical Intensity Modulation for Optical Vortex Beams with Orbital Angular Momentum

M.A. Yavorsky,[1] E.V. Barshak,[1,*] V.N. Berzhansky,[1] S.D. Lyashko,[1] M.A. Kozhaev,[1,2] A.Yu. Fedorov,[4,2] D.V. Vikulin,[1] and V.I. Belotelov[1,2,3]

[1] *V.I. Vernadsky Crimean Federal University, Vernadsky Prospekt 4, Simferopol 295007, Crimea*

[2] *Russian Quantum Center, Skolkovo, Moscow Region 143025, Russia*

[3] *Photonic and Quantum Technologies School, Lomonosov Moscow State University, Leninskie gori, Moscow 119991, Russia*

[4] *Moscow Institute of Physics and Technology, Dolgoprudny, Moscow Region 141701, Russia*

(Received 1 May 2022; revised 26 July 2022; accepted 19 September 2022; published 2 November 2022)

Here we theoretically and experimentally demonstrate a way to control the intensity of optical vortices by a magnetic field directed along the beam axis. We describe the principle of an optical vortex modulator and switch based on the Faraday effect in an iron garnet film. Importantly, the magnetic field influences only the polarization plane of the vortex and keeps its topological charge.

DOI: 10.1103/PhysRevApplied.18.054008

I. INTRODUCTION

Optical vortex beams (OVBs) [1] are characterized by a helicoidal shape of the wavefront with indefiniteness of the phase, which leads to the appearance of an orbital angular momentum (OAM) [2–5]. These unique properties of OVBs make them promising carriers of information encoded in additional orbital degrees of freedom of light [6]. In a simple case of Laguerre-Gaussian beams, OAM is defined as $\ell\hbar$ per photon, where $\hbar$ is the reduced Planck's constant and ℓ is a topological charge of the OVB. Since $\ell = 0, \pm 1, \pm 2, ..,$ a set of possible OAM values is theoretically unlimited, allowing one to increase communication-channel capacity by coding much more information as compared with the standard technologies based on non-OAM beams. Besides, it provides in principal another level of resistance to eavesdropping [7].

In this connection, much attention is paid to the control of OVBs. Various methods for generation and control of OVBs using optical crystals [8], q-plates [9], magnetic materials [10–13], special types of optical fibers [14–18], and photonic crystal fibers [19,20] have been proposed. One of the topical tasks of OVB-based data encoding is to find appropriate tools for the modulation of the OVB intensity. To date, intensity modulation is successfully implemented for the standard non-OAM-carrying (Gaussian) optical beams by usage of devices based on the magneto-optical (MO) effects in thin magnetic films. Such magnetic films are known to be widely used in design of MO modulators of optical beams [21–27], MO sensors [28–37], magnetometers [38,39], integrated MO devices [22,40–44], optical isolators, and other nonreciprocal optical devices [45–48].

Optimal chemical composition of MO films [49,50] allows one to increase the MO effects and get miniaturization of devices. In particular, one of the commonly applied MO materials is represented by films of bismuth-substituted iron garnet (BiIG). In this context, the perspective of MO control of vortex beams is attractive and looks promising. For example, quite recently, a MO dichroism effect [51] for OVBs has been demonstrated in a dysprosium BiIG film, which involves the dependence of the optical absorption on the sign of the topological charge of the OVB.

The idea of this paper is to show that the basic principles of MO modulation that are well established for non-OAM Gaussian beams can be directly generalized to OVBs. To this end, we theoretically and experimentally demonstrate the scheme of an intensity modulator and switch for vortex beams based on the Faraday rotation in a film of BiIG.

II. THEORETICAL BACKGROUNDS

We consider a scheme that is constructed from a polarizer P, a transparent BiIG film magnetized out of plane, and an analyzer A placed one after another, as depicted in Fig. 1. The analyzer has a transmission axis with an angle γ relative to the transmission axis of the polarizer. The BiIG film is described by the dielectric permittivity tensor

*lena.barshak@gmail.com

in the visible spectral range [21]:

$$\hat{\varepsilon}(M) = \begin{pmatrix} \varepsilon & i\delta\varepsilon(M) & 0 \\ -i\delta\varepsilon(M) & \varepsilon & 0 \\ 0 & 0 & \varepsilon \end{pmatrix}, \quad (1)$$

where the magnetically induced optical birefringence $\delta\varepsilon(M) << \varepsilon$, M is the magnetization of the BiIG film, and we assume that the field is uniform. The basis of linear polarizations $\mathbf{E} = (E_x, E_y, E_z)^T$ is used, where $\mathbf{E}$ is the electric field and T means transposition.

Let a monochromatic circularly polarized Laguerre-Gaussian beam of an arbitrary integer topological charge ℓ be normally incident on the BiIG film:

$$|\sigma, \ell, m\rangle = \mathbf{e}_\sigma \left(\frac{\sqrt{2}r}{w_0}\right)^{|\ell|} L_m^{|\ell|}\left(\frac{2r^2}{w_0^2}\right) e^{-(r/w_0)^2} e^{i\ell\varphi}. \quad (2)$$

Here $\mathbf{e}_\sigma$ is the unit vector of circular polarization, $\sigma = \pm 1$ means the right-hand and left-hand circular polarization, respectively, $L_m^{|\ell|}$ are the generalized Laguerre polynomials, m is the radial number, and w_0 is the beam waist.

As we show elsewhere, circularly polarized OVs (2) prove to be inherent eigenstates for the considered film with magnetically induced optical anisotropy. In other words, the incoming polarization state as well as the topological charge (and OAM) remain unchanged during the propagation. The optical beam in the BiIG film looks like

$$|\sigma, \ell, m\rangle(z) = \mathbf{e}_\sigma \frac{w_0}{w(z)} \left(\frac{\sqrt{2}r}{w(z)}\right)^{|\ell|} L_m^{|\ell|}\left(\frac{2r^2}{w^2(z)}\right) \times e^{-(r/w(z))^2} e^{i\sqrt{\varepsilon}k_0 z} e^{i\left(\ell\varphi - \alpha_\sigma z + \eta r^2 + \phi_G\right)}, \quad (3)$$

where $w(z) = w_0\sqrt{1 + (z/z_0)^2}$, $z_0 = \pi\sqrt{\varepsilon}w_0^2/\lambda$ is the Rayleigh distance, λ is a wavelength, $\alpha_\sigma = -\sigma k_0 \delta\varepsilon/2\sqrt{\varepsilon}$ is the standard Faraday term with vacuum wave number $k_0 = 2\pi/\lambda$, $\eta = k\sqrt{\varepsilon}/2R(z)$, $R(z) = z + z_0^2/z$ is the radius of the wavefront curvature, and ϕ_G is the Gouy phase [52]. Note that we have disregarded an insignificant to this study small phase correction that is due to optical spin-orbit interaction [53]. It should be noted that the separation of OAM from the circular polarization takes place, which can be ascertained straight from a comparison of Eqs. (2) and (3): the topological charge of the OVB passing through the film is conserved while the difference in phase velocities of orthogonal vortices is determined by the standard Faraday term α_σ.

In order to mathematically describe the light propagation in the scheme shown in Fig. 1, the Jones matrix formalism [54,55] can be used. According to this method, the state of a field should be represented as a decomposition over the eigenstates of the considered element. Thus, circularly polarized optical vortices with topological charge ℓ, which are eigenstates of the BiIG film, are considered as a basis. Strictly speaking, the generalization of the Jones formalism [56] to beams with additional orbital degree of freedom increases the dimension of the basis from 2 to 4, so the Jones vector is a 4×1 column vector $(a_{1,|\ell|,m}, a_{-1,|\ell|,m}, a_{1,-|\ell|,m}, a_{-1,-|\ell|,m})^T$ the components of which are weight coefficients of corresponding basis fields $|\pm 1, \pm|\ell|, m\rangle$. However, since the elements in the scheme shown in Fig. 1 only affect the spin part of the vortex, the description of total transformation of an OVB passing through the scheme is significantly simplified. Indeed, it turns out that the matrices of each element in Fig. 1 can be represented as a direct sum of matrices that act on subspaces of the orthogonal vectors with the same topological charge:

$$\{|1, \ell, m\rangle, |-1, \ell, m\rangle\}. \quad (4)$$

Thus, the matrix describing the beam propagation through the polarizer with a vertical transmission axis reads as

$$\hat{P}_0 = \hat{P}_0^{(+)} \oplus \hat{P}_0^{(-)}, \quad (5)$$

where $\hat{P}_0^{\pm} = \frac{1}{2}\begin{pmatrix} 1 & 1 \\ 1 & 1 \end{pmatrix}$ is defined for the vector subspace (4) and the superscript "±" indicates the sign of the topological charge of OVBs in the subspace.

The matrix for the BiIG film has the form of a diagonal phase matrix since it is determined over the basis of its eigenstates:

$$\hat{\tau}(\phi) = \hat{\tau}^{(+)}(\phi) \oplus \hat{\tau}^{(-)}(\phi), \quad (6)$$

where $\hat{\tau}^{(\pm)}(\phi) = \mathrm{diag}\left(e^{-i\phi}, e^{i\phi}\right)$, $\phi = k_0 d\delta\varepsilon(M)/2\sqrt{\varepsilon}$ is an angle of the Faraday rotation in the film of thickness d, and we have omitted the phase factor $e^{i\sqrt{\varepsilon}k_0 z} e^{i\left(\eta r^2 + \phi_G\right)}$.

The transformation of a beam passing through the analyzer with the transmission axis rotated at an angle γ with respect to the axis of the polarizer can be described as

$$\hat{P}_A(\gamma) = \hat{P}_A^{(+)}(\gamma) \oplus \hat{P}_A^{(-)}(\gamma), \quad (7)$$

where $\hat{P}_A^{(\pm)}(\gamma) = \hat{R}^{-1}(\gamma)\hat{P}_0^{(\pm)}\hat{R}(\gamma)$, $\hat{R}(\gamma) = \mathrm{diag}\left(e^{i\gamma}, e^{-i\gamma}\right)$ is a rotation matrix, and R^{-1} is the inverse matrix of R.

Hence, following the Jones method, the output field can be obtained from the input beam as

$$|\Psi\rangle_{\mathrm{out}} = \hat{P}_A(\gamma)\,\hat{\tau}(z, \phi)\,\hat{P}_0|\Psi\rangle_{\mathrm{in}} = \hat{\Omega}(\phi, \gamma)\,|\Psi\rangle_{\mathrm{in}}, \quad (8)$$

where $\hat{\Omega}(\phi, \gamma) = \hat{\Omega}^{(+)} \oplus \hat{\Omega}^{(-)}$, $\hat{\Omega}^{(\pm)} = (1/4)\begin{pmatrix} \Omega & \Omega \\ \Omega^* & \Omega^* \end{pmatrix}$, $\Omega = e^{-i\phi}\left(1 + e^{2i(\gamma+\phi)}\right)$, and Ω^* is Hermitian adjoint of Ω.

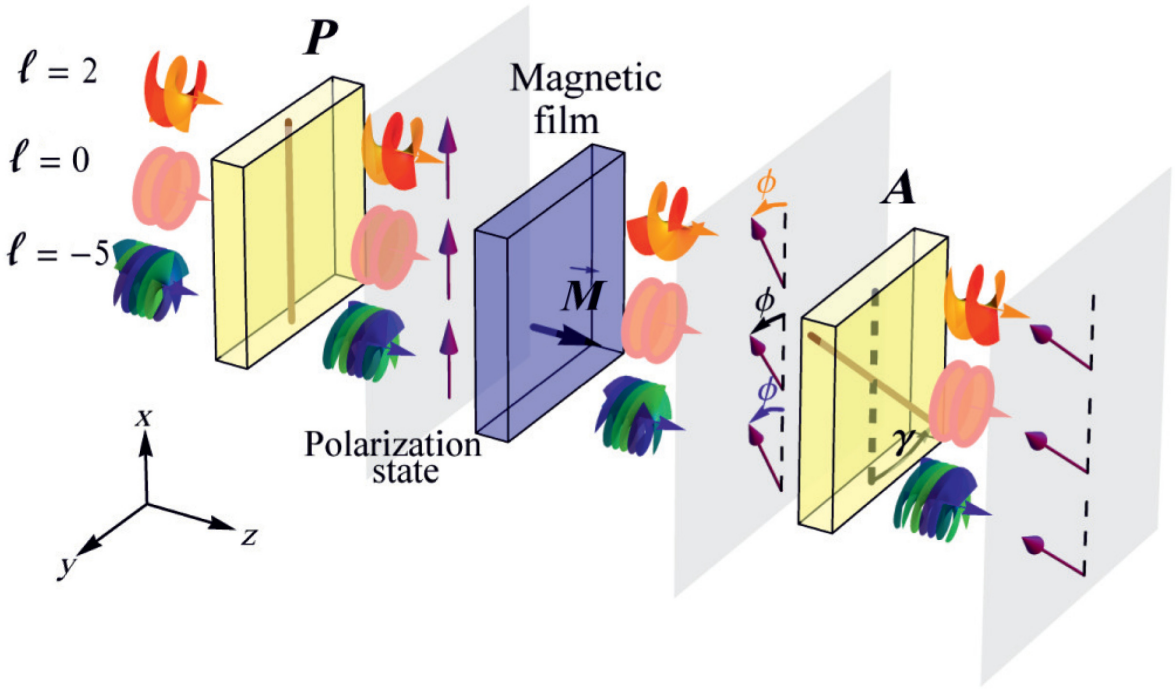

FIG. 1. Scheme of an intensity modulator for an OVB based on Faraday rotation in a BiIG film. The laser beam passes through polarizer P, BiIG film, and analyzer A, whose transmission axis has an angle γ with respect to that of the polarizer P. The topological charge of an input OVB is not changed. The polarization state of the OVB and the rotation of the linear polarization are depicted as an arrow near the OVB at each stage.

If the x-polarized OVB of topological charge ℓ is normally incident on the input of the scheme (see Fig. 1), an output field can be obtained according to Eq. (8):

$$|\Psi\rangle_{\text{out}} = \left[\frac{w_0}{w(z)}\left(\frac{\sqrt{2}r}{w(z)}\right)^{|\ell|} L_m^{|\ell|}\left(\frac{2r^2}{w^2(z)}\right) e^{-(r/w(z))^2} e^{i\sqrt{\varepsilon}k_0 z} \times e^{i\left(\ell\varphi+\eta r^2+\phi_G\right)} \cos(\gamma+\phi)\right]\begin{pmatrix}\cos\gamma\\ -\sin\gamma\end{pmatrix}. \tag{9}$$

The output OVB has the same topological charge as an input one, whereas its intensity calculated as the scalar product of the output field (9) with itself obeys the well-known Malus law, which for the normalized intensity (transmittance) reads as

$$T = \cos^2(\gamma+\phi). \tag{10}$$

Thus, we can conclude that if the BiIG film is used in the scheme shown in Fig. 1, Faraday rotation leads to a change in intensity of the OVB according to the Malus law in such a way as for zero-OAM beams. Whereas the OVB structure remains unchanged on passing through such a scheme, the Faraday effect allows one to modulate the intensity of the output beam by controlling the film magnetization M via the dependence $\delta\varepsilon(M)$. Depending on the value of the angle γ the intensity modulator and switch regimes can be implemented.

III. EXPERIMENT

In this section, we experimentally show the possibility of controlling the intensity of an OVB when passing through a thin epitaxial film of BiIG without destroying the vortex structure of the beam. A solid-state laser with a wavelength of 532 nm and adjustable power is used as a light source. First of all, it is necessary to obtain a stable OVB. To obtain this beam, a LCD modulator in the phase-intensity modulation mode is used. The resulting OVB is then isolated by a system of mirrors and diaphragms, after which it is analyzed using a CMOS camera. The obtained intensity distributions for a beam with topological charges from 1 to 5 are shown in Fig. 2.

It is impossible to unequivocally determine the topological charge and structure of the beam from the intensity pattern, so the interference method is used additionally. A modified scheme of a Mach-Zehnder interferometer is used, in which beam-splitting prisms with a ratio of 1:1 are used instead of translucent mirrors. The intensities of the main and reference beams are equalized using gray filters and then summed at the output beam splitter. The resulting interference pattern is recorded using a CMOS camera in real time, tracking possible changes in

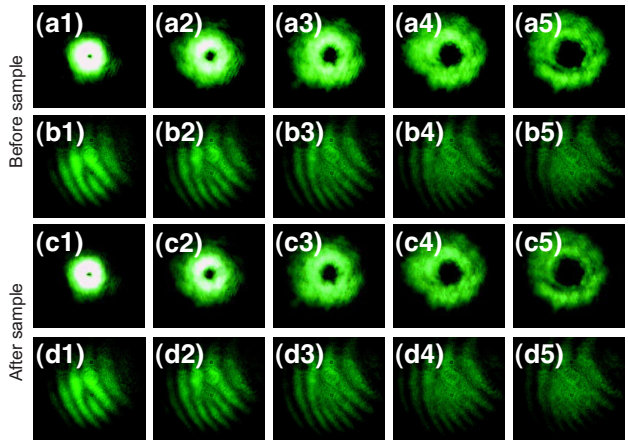

FIG. 2. Images of the intensity (a),(c) and interference pattern (b),(d) for the OVB with topological charges from 1 to 5 before (a),(b) and after (c),(d) the magnetic sample.

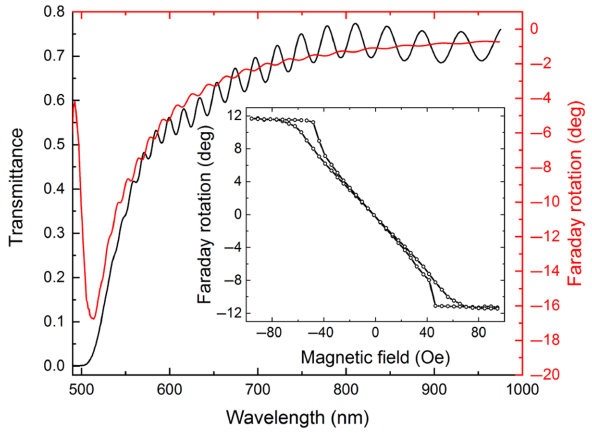

FIG. 3. Spectral dependencies of transmittance (black curve) and Faraday rotation (red curve) of the $(BiLuSm)_3(FeGa)_5O_{12}$ sample used for the experiment. Inset: hysteresis loop for the sample measured at 532 nm.

the vortex structure of the beam. Topological charge of the beam is defined as the difference in the number of interference fringes before and after the location of the singularity. To measure the integral intensity of the optical beam that passes through the sample, a Si photodetector is installed after the beam splitter located behind the sample. After visualizing the beam structure, we are ready to conduct measurements with the BiIG film. A sample of 4.2-μm-thick BiIG, $(BiLuSm)_3(FeGa)_5O_{12}$, is grown on a $Gd_3Ga_5O_{12}$ substrate with (111) orientation by liquid-phase epitaxy. To obtain a relatively large Faraday effect (Fig. 3, red curve), a significant amount of Bi ions is introduced into the film composition. For the sample used, the measured value of the Faraday rotation of the polarization plane is 14° with a relatively high transmission of 25% at a wavelength of 532 nm (Fig. 3, red and black curves). Relatively low values of the magnetic field required for the magnetic saturation of the sample in the out-of-plane direction are obtained by diamagnetic substitution of Fe ions with Ga ions, which also leads to the appearance of uniaxial anisotropy in the film. Measurements of the Faraday rotation hysteresis loop in an external out-of-plane magnetic field show a saturation field of 75 Oe (see inset to Fig. 3).

To modulate the intensity of the OVB passing through the magnetic sample, a Glan-Taylor polarizer is installed in front of the photodetector. Then the automatic system is used to find a crossed polarizers position by the minimum of the transmitted intensity to get the reference point. In this experiment, we test two regimes of OVB modulation: a MO switch and a MO intensity modulator. While for the switch application the angle between polarizer and analyzer is set equal to 90° (the crossed position), for the intensity modulator it is fixed at 45°. The Faraday rotation in the sample breaks the crossed polarization state, and the light begins to transmit to the photodetector. The transmittance is measured for optical beams with topological charges from 0 to 5 in the range of magnetic fields of ± 100 Oe.

The theoretical and experimental curves for the dependence of OVB transmittance on the external magnetic field are shown in Fig. 4 for the MO modulator [Fig. 4(a)] and MO switch [Fig. 4(b)] regimes. The theoretical curve is obtained from Eq. (10) accounting for the dependence of ϕ on magnetic field given by the hysteresis loop (Fig. 3). It should be stressed that in agreement with Eq. (10), the experimental points for different topological charges measured at a given magnetic field coincide with high accuracy. The inset to Fig. 4(a) confirms that a coefficient of light modulation $\Delta T/\Delta H$ does not depend on the topological charge. In the MO modulator regime light transmittance changes linearly with magnetic field for the field below saturating and, consequently, the coefficient of light modulation keeps constant. For the magnetic film used, the modulation amplitude is around 20% for magnetic field variation of 80 Oe. Obviously, for some thicker sample and a higher amplitude of magnetic field, a larger modulation depth can be achieved. However, in this work we aim to demonstrate a basic principle for modulation of OVBs and skip the optimization of the device.

In the MO switch regime, the transmittance of the OVB drops by two orders of magnitude down to 0.01% for near-zero magnetic field. In the case of optimization this dynamic range could be made larger.

A crucial point of the current experimental research is to confirm that application of a magnetic field does not influence the state of the OVB as theory predicts. Therefore, during the measurements, the topological charge of the OVB is controlled using an interference pattern. The obtained OVB images of topological charges from 1 to 5 and the corresponding interference patterns before and

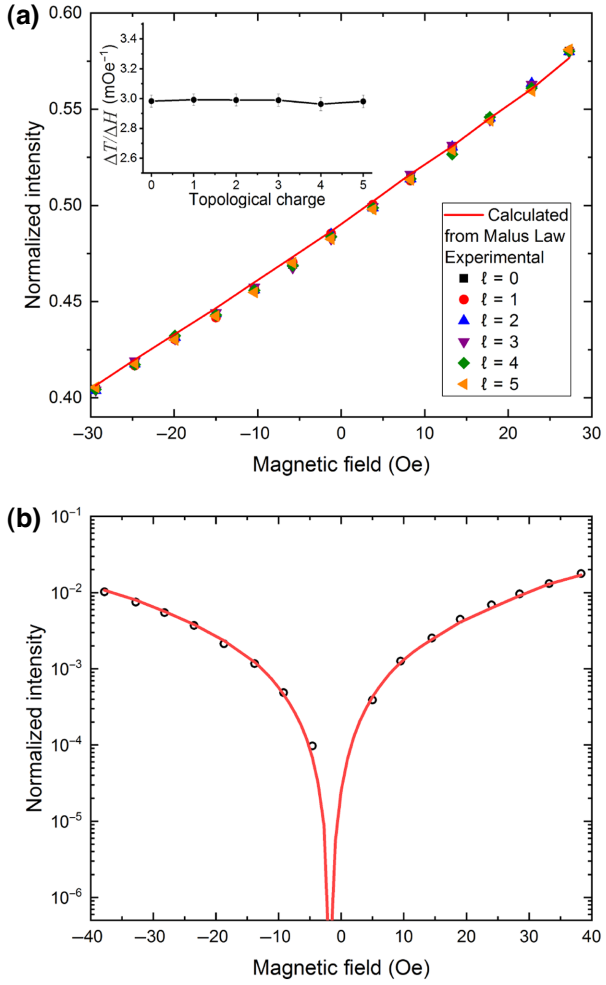

FIG. 4. Experimentally measured MO modulation of transmittance of optical beams with topological charge ℓ passing through a magnetic film. Solid curves represent theoretical results obtained from the Malus law (10). (a) The MO modulator regime. Experimental measurements are shown for the cases of topological charge from $\ell = 0$ to $\ell = 5$. Inset: coefficient of light modulation $\Delta T/\Delta H$ for different topological charges. (b) The MO switch regime. Experimental measurements are shown for the case of topological charge $\ell = 5$.

after placing the sample in the magnetic field do not differ (see Fig. 2). Any possible changes in the interference pattern are controlled both visually and by subtracting the OVB image without a magnetic field from the OVB image with an applied magnetic field. The results of the subtractions show that the interference pattern does not change at least within the accuracy of the registration noise of a CMOS camera, which confirms conservation of the topological charge upon transmission through the magnetized film. Consequently, the standard principles of light modulation based on the Faraday effect of Gaussian beams can be directly applied to the family of higher-order OVBs.

IV. CONCLUSION

To conclude, we theoretically and experimentally demonstrate the possibility of practical implementation of MO modulator and switch for OVBs with an arbitrary integer topological charge based on the standard methods of magneto-optical modulation. Magnetization of the sample does not spoil the state of the OVB. These results open a way for extension of the abilities of magneto-optics for the class of beams with an additional orbital degree of freedom of light, which could contribute to more miniature energy-efficient tools for controlling OAM-carrying beams for the needs of information technologies, micromanipulation, sensors, etc.

ACKNOWLEDGMENTS

The research is financially supported by the Russian Ministry of Education and Science, Megagrant (Project No. 075-15-2022-1108).

[1] S. Ramachandran and P. Kristensen, Optical vortices in fiber, Nanophotonics **2**, 455 (2013).
[2] Y. Shen, X. Wang, X. Zhenwei, C. Min, X. Fu, Q. Liu, M. Gong, and X. Yuan, Optical vortices 30 years on: OAM manipulation from topological charge to multiple singularities, Light. Sci. Appl. **8**, 90 (2019).
[3] R. Chen, H. Zhou, M. Moretti, X. Wang, and J. Li, Orbital angular momentum waves: Generation, detection, and emerging applications, IEEE Commun. Surv. Tutorials **22**, 840 (2020).
[4] M. J. Padgett, Orbital angular momentum 25 years on, Opt. Express **25**, 11265 (2017).
[5] A. M. Yao and M. J. Padgett, Orbital angular momentum: Origins, behavior and applications, Adv. Opt. Photon. **3**, 161 (2011).
[6] A. E. Willner, H. Huang, Y. Yan, Y. Ren, N. Ahmed, G. Xie, C. Bao, L. Li, Y. Cao, Z. Zhao, J. Wang, M. P. J. Lavery, M. Tur, S. Ramachandran, A. F. Molisch, N. Ashrafi, and S. Ashrafi, Optical communications using orbital angular momentum beams, Adv. Opt. Photon. **7**, 66 (2015).
[7] S. Franke-Arnold, S. Barnett, E. Yao, J. Leach, J. Courtial, and M. Padgett, Uncertainty principle for angular position and angular momentum, New J. Phys. **6**, 103 (2004).
[8] A. Yariv and P. Yeh, *Optical Waves in Crystals* (John Wiley & Sons, Inc., New York, 1984).
[9] N. Shitrit, S. Nechayev, V. Kleiner, and E. Hasman, Spin-dependent plasmonics based on interfering topological defects, Nano Lett. **12**, 1620 (2012).
[10] J. S. Woods, X. M. Chen, R. V. Chopdekar, B. Farmer, C. Mazzoli, R. Koch, A. S. Tremsin, W. Hu, A. Scholl, S. Kevan, S. Wilkins, W.-K. Kwok, L. E. De Long, S. Roy, and J. T. Hastings, Switchable X-Ray Orbital Angular Momentum from an Artificial Spin Ice, Phys. Rev. Lett. **126**, 117201 (2021).

[11] V. Karakhanyan, C. Eustache, Y. Lefier, and T. Grosjean, Inverse Faraday effect from the orbital angular momentum of light, Phys. Rev. B **105**, 045406 (2022).
[12] M. Fanciulli, M. Pancaldi, E. Pedersoli, M. Vimal, D. Bresteau, M. Luttmann, D. De Angelis, P. c. v. R. Ribič, B. Rösner, C. David, C. Spezzani, M. Manfredda, R. Sousa, I.-L. Prejbeanu, L. Vila, B. Dieny, G. De Ninno, F. Capotondi, M. Sacchi, and T. Ruchon, Observation of Magnetic Helicoidal Dichroism with Extreme Ultraviolet Light Vortices, Phys. Rev. Lett. **128**, 077401 (2022).
[13] N. Maccaferri, Y. Gorodetski, A. Toma, P. Zilio, F. De Angelis, and D. Garoli, Magnetoplasmonic control of plasmonic vortices, Appl. Phys. Lett. **111**, 201104 (2017).
[14] M. A. Yavorsky, All-fiber polarization-dependent optical vortex beams generation via flexural acoustic wave, Opt. Lett. **38**, 3151 (2013).
[15] C. Alexeyev, E. Barshak, Y. Fridman, and M. Yavorsky, Optical vortices in twisted elliptical fibres with torsional stress, Appl. Opt. **51**, 163 (2012).
[16] M. A. Yavorsky, E. V. Barshak, D. V. Vikulin, and C. N. Alexeyev, Spin-dependent OAM flipping in multihelical optical fibres, J. Opt. **20**, 115601 (2018).
[17] E. V. Barshak, C. N. Alexeyev, B. P. Lapin, and M. A. Yavorsky, Twisted anisotropic fibers for robust orbital-angular-momentum-based information transmission, Phys. Rev. A **91**, 033833 (2015).
[18] E. V. Barshak, D. V. Vikulin, B. P. Lapin, S. S. Alieva, C. N. Alexeyev, and M. A. Yavorsky, Robust higher-order optical vortices for information transmission in twisted anisotropic optical fibers, J. Opt. **23**, 035603 (2021).
[19] S. D. Lim, H. C. Park, I. K. Hwang, and B. Y. Kim, Combined effects of optical and acoustic birefringence on acousto-optic mode coupling in photonic crystal fiber, Opt. Exp. **16**, 6125 (2008).
[20] A. Diez, T. A. Birks, W. H. Reeves, B. J. Mangan, and P. S. J. Russell, Excitation of cladding modes in photonic crystal fibers by flexural acoustic waves, Opt. Lett. **25**, 1499 (2000).
[21] A. K. Zvezdin and V. A. Kotov, in *Modern Magnetooptics and Magnetooptical Materials* (Bristol: Institute of Physics Pub., 1997).
[22] G. Scott and D. Lacklison, Magnetooptic properties and applications of bismuth substituted iron garnets, IEEE Trans. Magn. **12**, 292 (1976).
[23] K. H. Chung, J. Heo, K. Takahashi, S. Mito, H. Takagi, J. Kim, P. B. Lim, and M. Inoue, Characteristics of magnetophotonic crystals based magneto-optic SLMs for spatial light phase modulators, J. Magn. Soc. Jpn. **32**, 114 (2008).
[24] V. N. Berzhansky, T. V. Mikhailova, A. V. Karavainikov, A. R. Prokopov, A. N. Shaposhnikov, I. N. Lukienko, Y. N. Kharchenko, O. V. Miloslavskaya, and N. F. Kharchenko, Microcavity one-dimensional magnetophotonic crystals with double layer iron garnet, J. Magn. Soc. Jpn. **36**, 42 (2012).
[25] K. Aoshima, N. Funabashi, K. Machida, Y. Miyamoto, K. Kuga, T. Ishibashi, N. Shimidzu, and F. Sato, Submicron magneto-optical spatial light modulation device for holographic displays driven by spin-polarized electrons, J. Disp. Technol. **6**, 374 (2010).
[26] K. Takahashi, F. Kawanishi, S. Mito, H. Takagi, K. H. Shin, J. Kim, P. B. Lim, H. Uchida, and M. Inoue, Study on magnetophotonic crystals for use in reflection-type magneto-optical spatial light modulators, J. Appl. Phys. **103**, 07B331 (2008).
[27] A. N. Kalish, D. O. Ignatyeva, V. I. Belotelov, L. E. Kreilkamp, I. A. Akimov, A. V. Gopal, M. Bayer, and A. P. Sukhorukov, Transformation of mode polarization in gyrotropic plasmonic waveguides, Laser Phys. **24**, 094006 (2014).
[28] J. E. Lenz, A review of magnetic sensors, Proc. IEEE **78**, 973 (1990).
[29] V. N. Berzhansky, A. V. Karavainikov, T. V. Mikhailova, A. R. Prokopov, A. N. Shaposhnikov, A. G. Shumilov, N. V. Lugovskoy, E. Y. Semuk, M. F. Kharchenko, I. M. Lukienko, Y. M. Kharchenko, and V. I. Belotelov, Nano- and micro-scale Bi-substituted iron garnet films for photonics and magneto-optic eddy current defectoscopy, J. Magn. Magn. Mater. **440**, 175 (2017).
[30] D. O. Ignatyeva, P. Kapralov, G. A. Knyazev, S. K. Sekatskii, G. Dietler, M. Nur-E-Alam, M. Vasiliev, K. E. Alameh, and V. I. Belotelov, High-Q surface modes in photonic crystal/iron garnet film heterostructures for sensor applications, JETP Lett. **104**, 679 (2016).
[31] O. V. Borovkova, D. O. Ignatyeva, S. K. Sekatskii, A. Karabchevsky, and V. I. Belotelov, High-Q surface electromagnetic wave resonance excitation in magnetophotonic crystals for supersensitive detection of weak light absorption in the near-infrared, Photon. Res. **8**, 57 (2020).
[32] N. Maccaferri, K. E. Gregorczyk, T. V. A. G. de Oliveira, M. Kataja, S. van Dijken, Z. Pirzadeh, A. Dmitriev, J. Akerman, M. Knez, and P. Vavassori, Ultrasensitive and label-free molecular-level detection enabled by light phase control in magnetoplasmonic nanoantennas, Nat. Commun. **6**, 6150 (2015).
[33] M. Manera, A. Colombelli, A. Taurino, A. Garcia-Martin, and R. Rella, Magneto-optical properties of noble-metal nanostructures: Functional nanomaterials for bio sensing, Sci. Rep. **8**, 12640 (2018).
[34] V. Bonanni, S. Bonetti, T. Pakizeh, Z. Pirzadeh, J. Chen, J. Nogues, P. Vavassori, R. Hillenbrand, J. Akerman, and A. Dmitriev, Designer magnetoplasmonics with nickel nanoferromagnets, Nano Lett. **11**, 5333 (2011).
[35] S. Pourjamal, M. Kataja, N. Maccaferri, P. Vavassori, and S. Dijken, Tunable magnetoplasmonics in lattices of Ni/SiO_2/Au dimers, Sci. Rep. **9**, 9907 (2019).
[36] T. Goto, A. V. Dorofeenko, A. M. Merzlikin, A. V. Baryshev, A. P. Vinogradov, M. Inoue, A. A. Lisyansky, and A. B. Granovsky, Optical Tamm States in One-Dimensional Magnetophotonic Structures, Phys. Rev. Lett. **101**, 113902 (2008).
[37] A. Chetvertukhin, A. Grunin, A. Baryshev, T. Dolgova, H. Uchida, M. Inoue, and A. Fedyanin, Magneto-optical Kerr effect enhancement at the Wood's anomaly in magnetoplasmonic crystals, J. Magn. Magn. Mater. **324**, 3516 (2012).
[38] S. Visnovsky, E. Liskova-Jakubisova, I. Harward, and Z. Celinski, Vector MO magnetometry for mapping microwave currents, AIP Adv. **8**, 056642 (2018).

[39] G. A. Knyazev, P. O. Kapralov, N. A. Gusev, A. N. Kalish, P. M. Vetoshko, S. A. Dagesyan, A. N. Shaposhnikov, A. R. Prokopov, V. N. Berzhansky, A. K. Zvezdin, and V. I. Belotelov, Magnetoplasmonic crystals for highly sensitive magnetometry, ACS Photonics **5**, 4951 (2018).

[40] X. Y. Sun, Q. Du, T. Goto, M. C. Onbasli, D. H. Kim, N. M. Aimon, J. Hu, and C. A. Ross, Single-step deposition of cerium-substituted yttrium iron garnet for monolithic on-chip optical isolation, ACS Photonics **2**, 856 (2015).

[41] D. Karki, R. El-Ganainy, and M. Levy, Toward High-Performing Topological Edge-State Optical Isolators, Phys. Rev. Appl. **11**, 034045 (2019).

[42] M. Levy, Nanomagnetic route to bias-magnet-free, on-chip Faraday rotators, J. Opt. Soc. Am. B **22**, 254 (2005).

[43] M. Inoue, M. Levy, and A. Baryshev, *Magnetophotonics: From Theory to Applications* (2013), p. XIII, 228.

[44] V. Belotelov and A. Zvezdin, Magnetooptics and extraordinary transmission of the perforated metallic films magnetized in polar geometry, J. Magn. Magn. Mater. **300**, e260 (2006). the third Moscow International Symposium on Magnetism 2005

[45] H. Takeda and S. John, Compact optical one-way waveguide isolators for photonic-band-gap microchips, Phys. Rev. A **78**, 023804 (2008).

[46] Z. Wang and S. Fan, Optical circulators in two-dimensional magneto-optical photonic crystals, Opt. Lett. **30**, 1989 (2005).

[47] R. Scarmozzino, M. Levy, I. Ilic, R. M. Osgood, R. Wolfe, C. J. Gutierrez, and G. A. Prinz, in *Conference on Lasers and Electro-Optics* (Optical Society of America, 1993), p. CWJ99.

[48] S. Kharratian, H. Urey, and M. Onbasli, RGB magnetophotonic crystals for high-contrast magnetooptical spatial light modulators, Sci. Rep. **9**, 644 (2019).

[49] A. Prokopov, P. Vetoshko, A. Shumilov, A. Shaposhnikov, A. Kuz'michev, N. Koshlyakova, V. Berzhansky, A. Zvezdin, and V. Belotelov, Epitaxial Bi-Gd-Sc iron-garnet films for magnetophotonic applications, J. Alloys Compd. **671**, 403 (2016).

[50] M. Nur-E-Alam, M. Vasiliev, V. Belotelov, and K. Alameh, Properties of ferrite garnet (Bi, Lu, $Y)_3(Fe, Ga)_5O_{12}$ thin film materials prepared by RF magnetron sputtering, Nanomaterials **8**, 355 (2018).

[51] A. Sirenko, P. Marsik, C. Bernhard, T. Stanislavchuk, V. Kiryukhin, and S. W. Cheong, Terahertz Vortex Beam as a Spectroscopic Probe of Magnetic Excitations, Phys. Rev. Lett. **122**, 237401 (2019).

[52] L. G. Gouy, Sur une propriété nouvelle des ondes lumineuses, C. R. Acad. Sci. Paris **110**, 1251 (1890).

[53] K. Y. Bliokh, F. J. Rodríguez-Fortuño, F. Nori, and A. V. Zayats, Spin–orbit interactions of light, Nat. Photonics **9**, 796 (2015).

[54] K. N. Alekseev and M. A. Yavorskii, Twisted optical fibers sustaining propagation of optical vortices, Opt. Spectrosc. **98**, 53 (2005).

[55] N. Ortega-Quijano and J. L. Arce-Diego, Generalized Jones matrices for anisotropic media, Opt. Exp. **21**, 6895 (2013).

[56] A. Voss, M. A. Ahmed, and T. Graf, Extension of the Jones matrix formalism to higher-order transverse modes, Opt. Lett. **32**, 83 (2007).